

# Probability distribution function for inclinations of merging compact binaries detected by gravitational wave interferometers

Naoki Seto

*Department of Physics, Kyoto University, Kyoto 606-8502, Japan*

21 October 2014

## ABSTRACT

We analytically discuss probability distribution function (PDF) for inclinations of merging compact binaries whose gravitational waves are coherently detected by a network of ground based interferometers. The PDF would be useful for studying prospects of (1) simultaneously detecting electromagnetic signals (such as gamma-ray-bursts) associated with binary mergers and (2) statistically constraining the related theoretical models from the actual observational data of multi-messenger astronomy. Our approach is similar to Schutz (2011), but we explicitly include the dependence of the polarization angles of the binaries, based on the concise formulation given in Cutler and Flanagan (1994). We find that the overall profiles of the PDFs are similar for any networks composed by the second generation detectors (Advanced-LIGO, Advanced-Virgo, KAGRA, LIGO-India). For example, 5.1% of detected binaries would have inclination angle less than  $10^\circ$  with at most 0.1% differences between the potential networks. A perturbative expression is also provided for generating the PDFs with a small number of parameters given by directional averages of the quantity  $\epsilon$  that characterises the asymmetry of network sensitivities to incoming two orthogonal polarization modes.

**Key words:** gravitational waves—binaries: close

## 1 INTRODUCTION

Gravitational waves (GWs) from merging neutron star binaries (NS-NSs) are the most promising targets of ground-based detectors. For the upcoming second generation interferometers, the estimated detection rate of NS-NSs is 1-100/yr, and it is likely that we can succeed to directly detect their GWs within five years (Abadie 2010). This estimated rate for NS-NSs is an order of magnitude higher than that for black hole-neutron star binaries (BH-NSs), which also have relevance to this paper.

Meanwhile, merging NS-NSs (and BH-NSs) are strong candidates for progenitors of short gamma ray bursts (SGRBs) (see *e.g.* Nakar 2007; Berger 2013). Reflecting geometry of the precedent inspiral phase, a merger product would have nearly axisymmetric profile around the direction  $\mathbf{l}$  of the orbital angular momentum of the binary (Metzger & Berger 2012). If the progenitor scenario for SGRBs is the case, jet like structures would be launched soon after the merger, toward the polar directions  $\pm\mathbf{l}$ , and they would be responsible for the observed gamma ray emissions. Later, more isotropic electromagnetic (EM) radiation might be emitted at lower energy band as recently discovered for GRB130603B (Tanvir et al. 2013; Berger, Fong & Chornock 2013; Hotokezaka et al. 2013).

Therefore, searches for EM signals triggered by GW detections of compact binary inspirals would become an exciting field of astronomy, and various possibilities have been actively discussed these days (see *e.g.* Fairhurst 2011; Schutz 2011; Cannon et al. 2012; Evans et al. 2012; LIGO Scientific Collaboration 2013; Nis-

sanke, Kasliwal & Georgieva 2013; Dietz et al. 2013; Kelley, Mandel & Ramirez-Ruiz 2013; Piran, Nakar & Rosswog 2013; Ghosh & Bose 2013; Kyutoku, Ioka & Shibata 2014; Arun et al. 2014; Kyutoku & Seto 2014). Given the expected axisymmetric profile of the merger products, it would be meaningful to evaluate the probability distribution function (PDF) of inclinations for compact binaries whose GWs are detected by the second generation detectors. Using the expected PDF, we can make statistical arguments about the future prospects for simultaneously detecting EM signals and constraining theoretical models based on observational data.

For a network of GW interferometers, the SNR of a binary depends on its sky direction  $\mathbf{n}$  and orientation  $\mathbf{l}$  (Cutler & Flanagan 1994; Sathyaprakash & Schutz 2009). Numerical studies by Monte Carlo simulations have been performed to properly deal with these multi-dimensional angular parameters (see *e.g.* Nissanke et al. 2010, 2013).

In this paper, we analytically study the PDFs of inclinations. Our underlying approach is similar to Seto (2014) in which the relative detection rates of merging binaries were formally examined for general networks of detectors, but with no attention to the PDFs of inclinations. Schutz (2011) discussed these two issues together, by introducing certain approximation to the dependence of the polarization angles  $\psi$  (explained in the next section) of binaries. But, for the PDFs of inclinations, the accuracy of this approximation has not been clarified so far. With the help of a concise expression provided by Cutler and Flanagan (1994), our analysis does not rely on the approximation and thus can be used to study validity of the

convenient method by Schutz (2011), as demonstrated below. Here the key quantity is  $\epsilon(\mathbf{n})$  which characterizes relative sensitivities of a network to two orthogonal polarization modes of incoming GWs.

Our analytical expressions derived in this paper are easily applicable to any networks of ground-based interferometers. We show that, in general, the PDFs depend weakly on networks, especially for nearly face-on binaries. This is because the emitted GW power is strongest to the face-on direction for which the quantity  $\epsilon(\mathbf{n})$  becomes less important, since the amplitudes of the two orthogonal polarization modes are nearly the same.

In contrast, for edge-on binaries, the PDFs depend strongly on  $\epsilon(\mathbf{n})$  and have largest scatters, when comparing different networks. However, the emitted GW power (and the detectable volume) is smallest for the edge-on binaries. Therefore, among the sample of the detected merging binaries, the relative fraction of the edge-on binaries is much smaller than the face-on binaries.

This paper is organized as follows. In Sec.2, we explain our basic formulation, assuming a coherent signal analysis for GWs from compact binary inspirals. We relate the total SNR and the expected detection rate of binaries. In Sec.3, we evaluate the PDF for inclinations of binaries at a given sky direction. In Sec.4, we discuss the full PDFs, including the angular averages with respect to sky directions. We also evaluate the PDFs concretely for the planned second-generation interferometers. Then we mention relative detection rates of merging binaries, in relation to Seto (2014). Sec.5 is devoted to a brief summary of this paper.

## 2 FORMULATION

### 2.1 Signal-to-Noise Ratio

Let us consider a binary at a sky direction  $\mathbf{n}$ . We use the unit vector  $\mathbf{l}$  for the orientation of its orbital angular momentum. This orientation vector is geometrically characterized by the two parameters  $\theta$  and  $\psi$ . Here the inclination angle  $\theta$  is the angle between  $\mathbf{n}$  and  $\mathbf{l}$ , and the polarization angle  $\psi$  fixes the rotational degree of freedom of  $\mathbf{l}$  around the line-of-sight  $\mathbf{n}$  (Cutler & Flanagan 1994; Sathyaprakash & Schutz 2009).

In the principle polarization frame of the binary, the two polarization modes  $+$  and  $\times$  of the mass-quadrupole waveform are proportional to  $d_+$  and  $d_\times$  given by

$$d_+(I) = \frac{I^2 + 1}{2}, \quad d_\times(I) = I \quad (1)$$

with  $I \equiv \cos \theta$  ( $I = 1$  for face-on and  $I = 0$  for edge-on; Peters & Mathews 1963). Below, we simply term  $I$  inclination. In astrophysical context, we are not interested in the sign of  $I$  and hereafter consider its absolute value (namely  $0 \leq I \leq 1$ ). Correspondingly, the inclination angle  $\theta$  is limited to the range  $0 \leq \theta \leq 90^\circ$  (identifying  $\pi - \theta \rightarrow \theta$ ). Throughout this paper, we neglect the precessions of orbital planes of binaries due to their spins. This would be a reasonable approximation for NS-NSs whose orbital angular momenta would dominate the spin angular momenta, due to their comparable masses and expected spin parameters much smaller than those of black holes (Cutler & Flanagan 1994; Apostolatos et al. 1994).

For detecting GWs from binaries, we consider to make coherent signal analysis using totally  $m$  ground-based interferometers with no correlated detector noises. Reflecting the spin-2 nature of GWs, the responses of each interferometer (labeled with  $i$ ) to the two polarization modes are written by

$$c_{i+}(\mathbf{n}, \psi) = a_i(\mathbf{n}) \cos 2\psi + b_i(\mathbf{n}) \sin 2\psi, \quad (2)$$

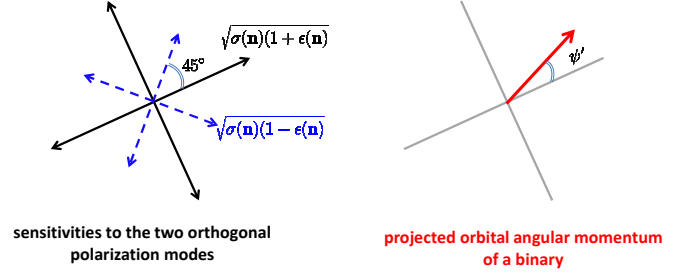


**Figure 1.** The geometric interpretation of Eq.(5) for incoming GW from a sky direction  $\mathbf{n}$ . (Left panel) In the plane normal to  $\mathbf{n}$ , the network has two orthogonal polarization bases at specific orientations, and measure these two modes with sensitivities proportional to  $\sqrt{\sigma(\mathbf{n})(1 + \epsilon(\mathbf{n}))}$  and  $\sqrt{\sigma(\mathbf{n})(1 - \epsilon(\mathbf{n}))}$ . Here the parameter  $\sigma(\mathbf{n})$  represents the total sensitivity to the two modes and  $\epsilon(\mathbf{n})$  shows the asymmetry between them. (Right panel) The orbital angular momentum of the binary is projected to the normal plane. Its orientation is characterised by the angle  $\psi'$  measured from the better sensitivity mode in the left panel. The original amplitudes (1) are given for the polarization modes symmetric to this projected vector.

$$c_{i\times}(\mathbf{n}, \psi) = -a_i(\mathbf{n}) \sin 2\psi + b_i(\mathbf{n}) \cos 2\psi. \quad (3)$$

The explicit forms of the functions  $a_i(\mathbf{n})$  and  $b_i(\mathbf{n})$  can be found in Schutz (2011) (see Eqs.(19) and (20) therein). Here the overall amplitude of  $(a_i, b_i)$  is proportional to the so-called horizon distance of the detector  $i$ .<sup>1</sup> But, below, we simply assume that all the interferometers have an identical noise curve with the same horizon distance. In practice, it is straightforward to take into account the differences of the horizon distances by setting appropriate weights for the functions  $(a_i, b_i)$ .

For the coherent signal analysis, the total signal-to-noise ratio (SNR) is obtained from Eqs.(1)-(3) and depends on the geometrical parameters  $(\mathbf{n}, I, \psi)$  as

$$SNR^2 \propto \sum_{i=1}^m [(c_{i+}d_+)^2 + (c_{i\times}d_\times)^2] \equiv f(\mathbf{n}, I, \psi) \quad (4)$$

(Cutler & Flanagan 1994; Dietz et al. 2013). Note that we only included the lowest quadrupole mode (1) for estimating the total SNR. This would be a good approximation for NS-NSs, since the next order correction is proportional to the mass difference and NS-NSs are expected to have similar masses, as commented earlier (Van Den Broeck & Sengupta 2007; Blanchet et al. 2008; Tagoshi et al. 2014). In Eq.(4), SNR is inversely proportional to the distance to the binary, while we omitted its explicit dependence.

With trigonometric relations (Cutler & Flanagan 1994), the  $\psi$ -dependence of  $f$  is simplified as

$$f(\mathbf{n}, \psi, I) = \sigma(\mathbf{n}) [D_0 + \epsilon(\mathbf{n}) D_1 \cos 4\psi'], \quad (5)$$

where the new polarization angle  $\psi' = \psi - \delta(\mathbf{n})$  is related to the original ones  $\psi$  with an offset  $\delta(\mathbf{n})$  that satisfies the following relation

<sup>1</sup> The horizon distance is the detectable range of a gravitational wave source that is optimally located and oriented. For a NS-NS binary of  $1.4M_\odot + 1.4M_\odot$  with the detection threshold of  $SNR = 8$ , each advanced-LIGO interferometer is planned to have the horizon distance of 445Mpc (Abadie et al. 2010). Advance-Virgo and KAGRA would have similar values.

$$\tan \delta(\mathbf{n}) = \frac{2 \sum_{i=1}^m a_i(\mathbf{n}) b_i(\mathbf{n})}{\sum_{i=1}^m (a_i(\mathbf{n})^2 - b_i(\mathbf{n})^2)}. \quad (6)$$

In Eq.(5), the functions  $D_0$  and  $D_1$  are defined by

$$D_0(I) \equiv (d_+^2 + d_\times^2) = \frac{I^4 + 6I^2 + 1}{4} \quad (7)$$

$$D_1(I) \equiv (d_+^2 - d_\times^2) = \frac{(I^2 - 1)^2}{4} \quad (8)$$

and the parameters  $\sigma$  and  $\epsilon$  are defined by

$$\sigma(\mathbf{n}) \equiv \sum_{i=1}^m a_i^2 + b_i^2 \quad (9)$$

$$\epsilon(\mathbf{n}) \equiv \frac{\sqrt{[\sum_{i=1}^m (a_i^2 - b_i^2)]^2 + 4(\sum_{i=1}^m a_i b_i)^2}}{\sigma(\mathbf{n})}. \quad (10)$$

From Cauchy-Schwartz inequality, we have

$$0 \leq \epsilon(\mathbf{n}) \leq 1. \quad (11)$$

The equality  $\epsilon(\mathbf{n}) = 1$  holds only when the vector  $(a_1(\mathbf{n}), \dots, a_m(\mathbf{n}))$  is parallel to  $(b_1(\mathbf{n}), \dots, b_m(\mathbf{n}))$ , including the case for a single detector network (with identity  $\epsilon(\mathbf{n}) = 1$  for all the directions  $\mathbf{n}$ ).

The geometric meaning of Eq.(5) is explained in Fig.1. The parameter  $\epsilon(\mathbf{n})$  characterizes the asymmetry of network sensitivity to the two orthogonal polarization modes given for each direction  $\mathbf{n}$  (Cutler & Flanagan 1994). This parameter plays an important role in this paper. With respect to the polarization decomposition shown in the left panel, the amplitudes of the quadrupole waves of the binary (with the projected angle  $\psi'$ ) are given by

$$(d_+^2 \cos^2 2\psi' + d_\times^2 \sin^2 2\psi')^{1/2} \quad (12)$$

and

$$(d_+^2 \sin^2 2\psi' + d_\times^2 \cos^2 2\psi')^{1/2} \quad (13)$$

with  $d_+$  and  $d_\times$  defined by Eq.(1). Then we have

$$\begin{aligned} \text{SNR}^2 &\propto \sigma(\mathbf{n})(1 + \epsilon(\mathbf{n})) (d_+^2 \cos^2 2\psi' + d_\times^2 \sin^2 2\psi') \\ &\quad + \sigma(\mathbf{n})(1 - \epsilon(\mathbf{n})) (d_+^2 \sin^2 2\psi' + d_\times^2 \cos^2 2\psi'). \end{aligned}$$

The right-hand-side of this relation is identical to that of Eq.(5).

For a face-on binary  $I = 1$ , we have  $d_+ = d_\times$  (thus  $D_1 = 0$ ) and this expression does not depend on the angle  $\psi'$  (and  $\epsilon$ ). On the other hand, edge-on binaries ( $I = 0$ ) emit 100% linearly polarized GWs and Eq.(5) depends strongly on  $\epsilon(\mathbf{n})$  and  $\psi'$  with  $D_0 = D_1 = 1/4$ .

## 2.2 Detectable Binaries

We define  $r_{\max}$  as the maximum distances to the binaries detectable above a given SNR threshold. Then, from Eq.(4), we have a scaling relation

$$r_{\max} \propto f(\mathbf{n}, I, \psi)^{1/2} \quad (14)$$

(Finn & Chernoff 1993; Schutz 2011; Dietz et al. 2013). Therefore, assuming that merging binaries have random orientations and spatial distributions, the expected number of detectable ones in a parameter range  $d\mathbf{n}dI d\psi$  is proportional to

$$f(\mathbf{n}, I, \psi)^{3/2} d\mathbf{n}d\psi dI. \quad (15)$$

Here we neglected cosmological effects that would be unimportant at least for NS-NSs observed with second generation detectors. In this paper, we study the PDFs in appropriately normalized forms. Therefore the actual values of the horizon distance and the comoving merger rate are irrelevant to our results.

Next we integrate out the less interesting polarization parameter  $\psi$  and define the new function  $\alpha(\mathbf{n}, I)$  by

$$\alpha(\mathbf{n}, I) \equiv \frac{2}{\pi} \int_0^{\pi/2} f(\mathbf{n}, I, \psi)^{3/2} d\psi. \quad (16)$$

As we initially integrate the polarization angle  $\psi$  (or equivalently  $\psi'$ ) before integrating the sky direction  $\mathbf{n}$ , we actually do not need to directly handle the complicated offset  $\delta(\mathbf{n})$ . This is an advantageous point of our approach, and simplifies the actual evaluation of PDFs.

From Eq.(5), the integral  $\alpha(\mathbf{n}, I)$  can be formally expressed as

$$\alpha(\mathbf{n}, I) = \sigma(\mathbf{n})^{3/2} D_0(I)^{3/2} \gamma[\epsilon(\mathbf{n}) R(I)], \quad (17)$$

where we define

$$R(I) \equiv \left( \frac{D_1}{D_0} \right) = \frac{(I^2 - 1)^2}{I^4 + 6I^2 + 1} \quad (18)$$

and

$$\gamma(x) \equiv \frac{2}{\pi} \int_0^{\pi/2} (1 + x \cos 4\psi)^{3/2} d\psi. \quad (19)$$

The integral  $\gamma(x)$  is given as follows

$$\gamma(x) = \frac{2(1-x)^{1/2}}{3\pi} \left[ 4E\left(\frac{2x}{x-1}\right) - (1+x)K\left(\frac{2x}{x-1}\right) \right] \quad (20)$$

with the incomplete elliptic integral of the second kind  $E(x)$  and the complete elliptic integral of the first kind  $K(x)$  defined respectively by

$$E(x) \equiv \int_0^{\pi/2} (1 - x \sin^2 \theta)^{1/2} d\theta \quad (21)$$

$$K(x) \equiv \int_0^{\pi/2} (1 - x \sin^2 \theta)^{-1/2} d\theta \quad (22)$$

(see also Dietz et al. 2013).

Around  $x = 0$ , the integral  $\gamma(x)$  is expanded as follows;

$$\begin{aligned} \gamma(x) &= 1 + \frac{3}{16}x^2 + \frac{9}{1024}x^4 + \frac{35}{16384}x^6 + \frac{3465}{4194304}x^8 \\ &\quad + \frac{27027}{67108864}x^{10} + \frac{969969}{4294967296}x^{12} + O(x^{14}). \end{aligned} \quad (23)$$

We use this expression later in Sec.4.

Finally, after integrating the sky direction  $\mathbf{n}$  of binaries, the PDF for a network can be formally expressed as

$$P_{\text{net}}(I) = \frac{\int_{4\pi} d\mathbf{n} \alpha(\mathbf{n}, I)}{\int_0^1 dI \int_{4\pi} d\mathbf{n} \alpha(\mathbf{n}, I)}. \quad (24)$$

Here the denominator is a normalization factor to realize

$$\int_0^1 P_{\text{net}}(I) dI = 1. \quad (25)$$

### 2.3 Total Detection Rate

Our formulation up to Eq.(15) is similar to Seto (2014) in which the relative detection rates of binaries were examined by integrating all the angular variables including  $I$ , without paying attention to its PDF.

In this subsection, we define the following quantity

$$X \equiv \int_0^1 dI \int_{4\pi} d\mathbf{n} \alpha(\mathbf{n}, I), \quad (26)$$

and briefly summarize the arguments in Seto (2014). Here we only extracted geometrical information relevant for the relative detection rates, considering comparisons between different networks. Actually, the integral (26) for the relative rates is identical to the denominator in Eq.(24).

For a hypothetical network with  $\epsilon(\mathbf{n}) = 0$ , the function  $\alpha(\mathbf{n}, I)$  becomes a separable form as  $\sigma(\mathbf{n})^{3/2} D_0(I)^{3/2}$  and we have

$$X_0 \equiv \int_0^1 dI D_0(I)^{3/2} \int_{4\pi} d\mathbf{n} \sigma(\mathbf{n})^{3/2} = N_0 \int_{4\pi} d\mathbf{n} \sigma(\mathbf{n})^{3/2} \quad (27)$$

with the parameter  $N_0 \equiv 0.82155$ . This expression can be easily evaluated and we do not need to directly deal with the dependence on the orientation angles  $(I, \psi)$  of binaries. Therefore, as a convenient approximation to the original complicated one  $X$ , we might use  $X_0$  for general networks with  $\epsilon(\mathbf{n}) \neq 0$ . Indeed, the expression  $X_0$  is essentially the same as that proposed by Schutz (2011) for estimating the relative rates.

The question here is how well the original integral  $X$  is reproduced by the approximation  $X_0$ . In order to check this, we define the ratio

$$Y \equiv \frac{X}{X_0}. \quad (28)$$

The main result in Seto (2014) is the following relation

$$Y = \frac{\int_{4\pi} d\mathbf{n} \sigma(\mathbf{n})^{3/2} G[\epsilon(\mathbf{n})]}{\int_{4\pi} d\mathbf{n} \sigma(\mathbf{n})^{3/2}} \quad (29)$$

where  $G(x)$  is a monotonically increasing function of  $x$  and perturbatively expanded as

$$G(x) = 1 + 0.00978x^2 + 0.00026x^4 + O(x^6) \quad (30)$$

with  $G(0) = 1$  and  $G(1) = C_{01} \equiv 1.010125$ .

Given the inequality  $\sigma(\mathbf{n}) \geq 0$ , we generally have the bounds

$$1 \leq Y \leq 1.010125. \quad (31)$$

Therefore the simple expression  $X_0$  is an excellent approximation to  $X$ . These inequalities would be practically sufficient for astronomical arguments, but, we can actually evaluate the ratio  $Y$ , as a byproduct of our perturbative formulation. This will be discussed in Sec.4.5.

### 3 PDFS FOR GIVEN SKY DIRECTIONS

In this section, we discuss the PDFs of inclinations  $I$  for a fixed parameter  $\epsilon$ , without taking the sky average as in Eq.(24). From Eq.(17), we define the function  $P(I, \epsilon)$  as follows

$$P(I, \epsilon) = \frac{D_0(I)^{3/2} \gamma[\epsilon R(I)]}{N_\epsilon} \quad (32)$$

with the normalization factor

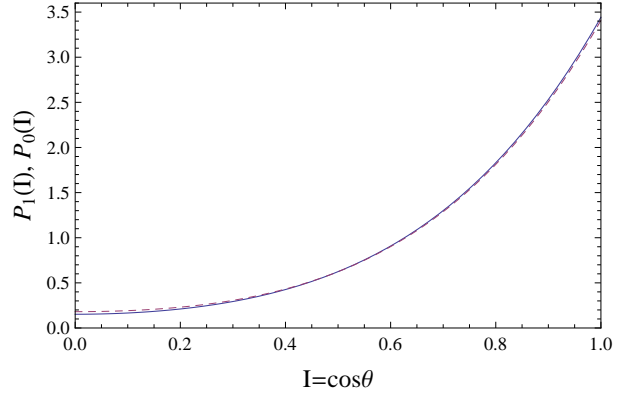


**Figure 2.** The functions  $P(I, \epsilon)$  for  $\epsilon = 0$  and 1. The solid curve represents  $P_0(I) = P(I, 0)$  and the dashed one is for  $P_1(I) = P(I, 1)$ . The latter is identical to the sky averaged PDF for a single detector.

$$N_\epsilon = \int_0^1 dI D_0(I)^{3/2} \gamma[\epsilon R(I)]. \quad (33)$$

The function  $P(I, \epsilon)$  ( $0 \leq \epsilon \leq 1$ ) can be regarded as the PDF for a given sky direction  $\mathbf{n}$  with  $\epsilon(\mathbf{n}) = \epsilon$ . In addition, for the special value  $\epsilon = 1$ , it corresponds to the full (sky averaged) PDF for a network composed by a single interferometer that identically has  $\epsilon(\mathbf{n}) = 1$ , as mentioned earlier. Our primary task in this section is to explicitly demonstrate that the function  $P(I, \epsilon)$  does not have strong dependence on  $\epsilon$ .

To begin with, we introduce the notations  $P_0(I)$  and  $P_1(I)$  for the two boundary parameters  $\epsilon = 0$  and 1 by

$$P_0(I) \equiv P(I, 0) = \frac{D_0(I)^{3/2}}{N_0} \quad (34)$$

$$P_1(I) \equiv P(I, 1) = \frac{D_0(I)^{3/2}}{N_1} \gamma[R(I)] \quad (35)$$

with the normalization factors  $N_0 = 0.82155$  (already appeared in Eq.(27)) and  $N_1 = 0.82986$ . We have  $N_1/N_0 = C_{01} = 1.010125$ .

Schutz (2011) studied the PDF of inclinations for detected binaries. He used an approximation in which the explicit  $\psi$  dependence was not included for the effective volume (5). In our language, this treatment corresponds to commute the order of the following two operations in Eq.(16); (i) the nonlinear manipulation  $[\cdot \cdot \cdot]^{3/2}$  and (ii) the  $\psi$ -averaging. It is equivalent to taking  $\epsilon(\mathbf{n}) = 0$  in Eq.(17). Consequently, his PDF is identical to  $P_0(I)$  defined in Eq.(34). In this paper, we can analytically show that this PDF generally serves as a good approximation, irrespective of the details of a network.

In Fig.2 we present  $P_0(I)$  (solid curve) and  $P_1(I)$  (dashed curve). The two curves show similar shapes. In order to enhance the differences between them, we show the ratio  $P_1(I)/P_0(I)$  (dashed curve) in Fig.3, together with  $P(I, \epsilon)/P_0(I)$  at the intermediate values  $\epsilon = 0.1, 0.2, \dots, 0.9$  (solid curves).

For a given  $\epsilon$ , the function  $P(I, \epsilon)$  becomes minimum at  $I = 0$ , reflecting the smallest amplitude at the edge-on configuration. At the same time, as shown in Fig.3, the ratios  $P(I, \epsilon)/P_0(I)$  show the largest scatter at  $I = 0$ . This is because the emitted waves are 100% linearly polarized and the effects of the asymmetry parameter  $\epsilon$  become significant.

**Table 1.** The cumulative PDF:  $[\mathcal{P}_{cum}(\theta, 0) + \mathcal{P}_{cum}(\theta, 1)]/2$  at sample points.

$\theta$	$1^\circ$	$5^\circ$	$10^\circ$	$20^\circ$	$45^\circ$	$80^\circ$
cumulative PDF	$5.2 \times 10^{-4}$	0.013	0.051	0.19	0.66	0.969

In contrast, at the face-on configuration  $I = 1$ , we obtain  $R(I) = 0$  and  $\gamma(\epsilon R(I)) = 1$ . Therefore, around  $I \sim 1$ , we approximately have

$$P(I, \epsilon) \simeq \frac{D_0(I)^{3/2}}{N_\epsilon} \quad (36)$$

with  $P(I, \epsilon)/P_0(I) \simeq N_0/N_\epsilon$  that is now a decreasing function of  $\epsilon$  with the minimum value  $N_0/N_1 = 1/C_{01} = 0.99$  at  $\epsilon = 1$ . This shows that, around  $I \sim 1$ , the relative difference between  $P(I, \epsilon)$  is at most  $\sim 1\%$ .

As shown in Fig.3, the two functions  $P_0(I)$  and  $P_1(I)$  intersect at  $I = 0.489$  where the family  $P(I, \epsilon)$  depends very weakly on  $\epsilon$ . Except the tiny region around this intersection, the function  $P(I, \epsilon)$  ( $0 \leq \epsilon \leq 1$ ) is bounded by the two curves  $P_0(I)$  and  $P_1(I)$ . In the next section, we apply this result for discussing the overall profile of the sky-averaged function  $P_{net}(I)$ .

So far, we have studied the PDFs for  $I$  only in a differential form. Here we examine the cumulative PDFs  $\mathcal{P}_{cum}(\theta, \epsilon)$  for the inclination angle  $\theta = \cos^{-1} I$  defined by

$$\mathcal{P}_{cum}(\theta, \epsilon) \equiv \int_{\cos \theta}^1 P(I, \epsilon) dI \quad (37)$$

with  $0 \leq \theta \leq 90^\circ$ . This function represents the probability that a detected binary has a viewing angle less than  $\theta$ , from its symmetry axis  $\mathbf{l}$ . In this cumulative form, we rigidly have the following bounds

$$\mathcal{P}_{cum}(\theta, 1) \leq \mathcal{P}_{cum}(\theta, \epsilon) \leq \mathcal{P}_{cum}(\theta, 0) \quad (38)$$

and the two boundaries have small relative differences

$$1 \leq \mathcal{P}_{cum}(\theta, 0)/\mathcal{P}_{cum}(\theta, 1) \leq C_{01} = 1.010125. \quad (39)$$

We can confirm their similarity in Fig.4. The tight confinement (38) would become useful in the next section.

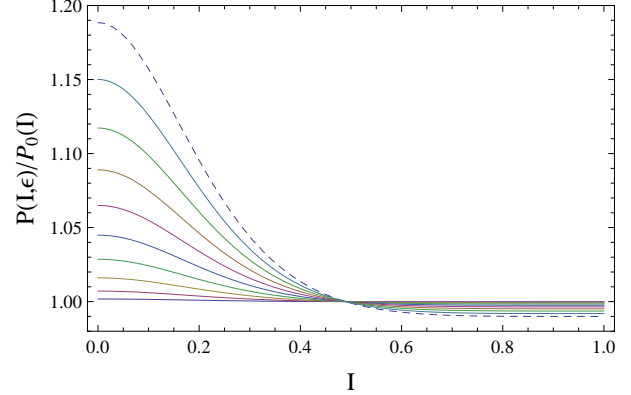
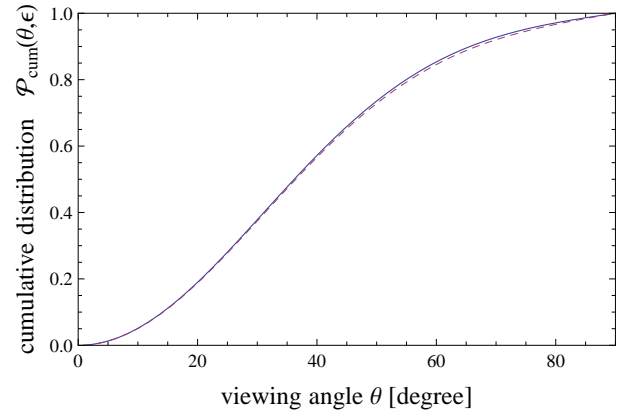
For conveniences at astronomical studies, we provide a fitting function for  $\mathcal{P}_{cum}(\theta, \epsilon)$

$$\begin{aligned} \mathcal{P}_{cum,f}(\theta) = & 4.23888 \left( \frac{\theta}{90^\circ} \right)^2 - 0.373208 \left( \frac{\theta}{90^\circ} \right)^3 \\ & - 6.64160 \left( \frac{\theta}{90^\circ} \right)^4 \end{aligned} \quad (40)$$

which reproduces the functions  $\mathcal{P}_{cum}(\theta, \epsilon)$  ( $0 \leq \epsilon \leq 1$ ) with relative error less than 1% in the range  $0 \leq \theta \leq 30^\circ$ . In Table.1, we also evaluate the mean  $[\mathcal{P}_{cum}(\theta, 0) + \mathcal{P}_{cum}(\theta, 1)]/2$  for some representative angles  $\theta$ .

#### 4 ALL SKY DISTRIBUTION

In this section, we discuss the full (sky averaged) functions  $P_{net}(I)$  defined in Eq.(24) for various networks of ground-based interferometers. In Sec.4.1 we first mention their overall profiles based on the results shown in the previous section. Then, in Sec.4.2, we use the perturbative expansion (23) and derive an expression for more precisely evaluating  $P_{net}(I)$ . The validity of our perturbative method is examined in Sec.4.3. In Sec.4.4, we apply our

**Figure 3.** The ratios  $P_1(I)/P_0(I)$  (dashed curve) and  $P(I, \epsilon)/P_0(I)$  with  $\epsilon = 0.1, 0.2, \dots, 0.9$  (solid curves from bottom to top). At  $I = 0$ , the ratio  $P(I, \epsilon)/P_0(I)$  is an increasing function of  $\epsilon$ . The two function  $P_1(I)$  and  $P_0(I)$  intersect at  $I = 0.489$ .**Figure 4.** The cumulative functions  $\mathcal{P}_{cum}(\theta, \epsilon)$  for  $\epsilon = 0$  (solid curve) and 1 (dashed curve). Their relative difference is only  $\sim 1\%$ . For  $0 \leq \epsilon \leq 1$ , the function  $\mathcal{P}_{cum}(\theta, \epsilon)$  is tightly bounded by these two curves.

method for networks composed by second generation interferometers. In Sec.4.5, we mention the relative detection rates of merging binaries, in relation to Seto (2014) and Sec.2.3.

#### 4.1 general remarks

From Eqs.(17) and (24), the function  $P_{net}(I)$  is obtained by taking an average of  $P[I, \epsilon(\mathbf{n})]$  with the following relative weights

$$d\mathbf{n} \sigma(\mathbf{n})^{3/2} N_\epsilon(\mathbf{n}). \quad (41)$$

Therefore, similar to the previous one  $P(I, \epsilon)$ , the averaged one  $P_{net}(I)$  should be bounded by the two functions  $P_0(I)$  and  $P_1(I)$  except the tiny region around their intersection at  $I = 0.489$ , as mentioned earlier in Fig.3. This means that the overall profile of  $P_{net}(I)$  can be approximately understood from the shapes of the two functions  $P_0(I)$  and  $P_1(I)$ . Around  $I \sim 1$ , the function  $P_{net}(I)$  weakly depends on the details of a network (see Fig.3). Among the binaries detected by a single interferometer, the fraction of nearly edge-on ones ( $I \sim 0$ ) could be at most  $\sim 20\%$  larger than a network with multiple interferometers.

Next, we discuss the cumulative PDFs for networks. As in Eq.(37), we define  $\mathcal{P}_{cum,net}(\theta)$  by

$$\mathcal{P}_{cum,net}(\theta) \equiv \int_{\cos \theta}^1 P_{net}(I) dI. \quad (42)$$

By changing the order of the integrals  $d\mathbf{n}$  and  $dI$ , we can understand that the function  $\mathcal{P}_{cum,net}(\theta)$  is obtained by averaging  $\mathcal{P}_{cum}[\theta, \epsilon(\mathbf{n})]$  again with the weight (41). Since the cumulative PDFs  $\mathcal{P}_{cum}[\theta, \epsilon(\mathbf{n})]$  are tightly bounded by the two functions  $\mathcal{P}_{cum}(\theta, 0)$  and  $\mathcal{P}_{cum}(\theta, 1)$ , the sky averaged one  $\mathcal{P}_{cum,net}(\theta)$  must be also bounded by them. Therefore, with relative error less than  $\sim 1\%$ , we can apply the previous fitting formula (40) for the sky averaged one  $\mathcal{P}_{cum,net}(\theta)$  in the range  $0 \leq \theta \leq 30^\circ$ , irrespective of the details of networks. Similarly, we can apply Table.1 for given networks.

For example,  $\sim 5\%$  of detected binaries have viewing angle  $\theta$  less than  $10^\circ$ . The fraction becomes  $\sim 1.3\%$  for  $\theta \leq 5^\circ$ . In other words, if one hundred binaries are detected by a network, the minimum inclination angle would be  $\theta \sim 5^\circ$  and we will have  $\sim 5$  binaries with  $\theta$  less than  $10^\circ$ .

## 4.2 perturbative evaluation

Now we move to develop a perturbative method for evaluating  $P_{net}(I)$  more precisely. First we rewrite  $P_{net}(I)$  as follows

$$P_{net}(I) = \frac{Q_{net}(I)}{M_{net}}, \quad (43)$$

where the numerator and the denominator are non-dimensional quantities defined by

$$Q_{net}(I) = \frac{\int_{4\pi} d\mathbf{n} \alpha(\mathbf{n}, I)}{\int_{4\pi} d\mathbf{n} \sigma(\mathbf{n})^{3/2}}, \quad M_{net} = \frac{\int_0^1 dI \int_{4\pi} d\mathbf{n} \alpha(\mathbf{n}, I)}{\int_{4\pi} d\mathbf{n} \sigma(\mathbf{n})^{3/2}}. \quad (44)$$

Here we introduced the common factor  $[\int_{4\pi} d\mathbf{n} \sigma(\mathbf{n})^{3/2}]^{-1}$  to make our analysis comprehensive. Applying the expansion (23) for  $Q_{net}(I)$ , we obtain

$$Q_{net}(I) = D_0(I)^{3/2} \left( 1 + \frac{3R^2 s_2}{16} + \frac{9R^4 s_4}{1024} + \frac{35R^6 s_6}{16384} + \dots \right) \quad (45)$$

with a function  $R(I)$  defined in Eq.(18) and the coefficients  $s_j$  given by

$$s_j \equiv \frac{\int_{4\pi} \sigma(\mathbf{n})^{3/2} \epsilon(\mathbf{n})^j d\mathbf{n}}{\int_{4\pi} \sigma(\mathbf{n})^{3/2} d\mathbf{n}}. \quad (46)$$

From the inequalities  $0 \leq \epsilon(\mathbf{n}) \leq 1$ , we have

$$0 \leq s_{j+1} \leq s_j \leq 1 \quad (47)$$

with the equality  $s_j = s_{j+1}$  only for  $s_j = 0$  (identically  $\epsilon(\mathbf{n}) = 0$ ) or  $s_j = 1$  (identically  $\epsilon(\mathbf{n}) = 1$ ). In our perturbative approach, all the information of a network is projected into the sequence of numbers  $(s_2, s_4, s_6, \dots)$ . We thus call them network parameters.

In the same manner, the normalization factor  $M_{net}$  can be perturbatively evaluated as

$$M_{net} = N_0 + \frac{3}{16} u_2 s_2 + \frac{9}{1024} u_4 s_4 + \frac{35}{16384} u_6 s_6 + \dots \quad (48)$$

where we define the parameters  $u_j$  given by the following integrals

$$u_j \equiv \int_0^1 D_0(I)^{3/2} R(I)^j dI. \quad (49)$$

**Table 2.** The parameters defined in Eq.(49).

$u_2$	$u_4$	$u_6$	$u_8$	$u_{10}$	$u_{12}$
0.042885	0.024136	0.018303	0.015297	0.013400	0.012067

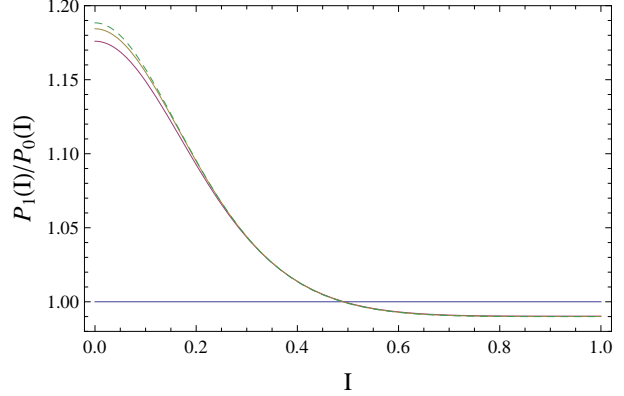


**Figure 5.** The ratio  $P_1(I)/P_0(I)$  (dashed curve) and its perturbative expansions according to Eq.(50) (0th, 2nd and 4th order approximations: solid curves from bottom). Convergence of the perturbative expansion is fast.

These are constants and do not depend on networks. In Table.2, we present them up to  $u_{12}$ .

## 4.3 expansion for a single detector network

In the previous subsection, we explained how to perturbatively evaluate the sky averaged function  $P_{net}(I)$ . Our expression (43) is characterized by the network parameters  $(s_2, s_4, \dots)$  with  $0 \leq s_j \leq 1$ . From Eqs.(45) and (48), we will have better convergence for smaller  $s_j$ . On the other hand, the convergence would become worst for the maximum value  $s_j = 1$ , corresponding to a single detector network. But, for this case, we actually have the non-perturbative result  $P_1(I)$  given in Eq.(35). Therefore, we can test the validity of our perturbative expansion by comparing the two results.

For  $s_j = 1$ , our perturbative expression is given by

$$P_1(I) = D_0(I)^{3/2} \frac{1 + \frac{3}{16} R^2 + \frac{9}{1024} R^4 + \frac{35}{16384} R^6 + \dots}{N_0 + \frac{3}{16} u_2 + \frac{9}{1024} u_4 + \frac{35}{16384} u_6 + \dots}. \quad (50)$$

In Fig.5, we show the non-perturbative results (dashed curve) and the 0th, 2nd and 4th order approximations (solid curves). This figure shows that, even in the worst case  $s_j = 1$ , the convergence is fast and the relative error is at most  $\sim 0.3\%$  with the 4th order approximation. Therefore, our perturbative method would be efficient to reproduce the function  $P_{net}(I)$ .

## 4.4 second generation detector networks

Now we concretely evaluate the averaged function  $P_{net}(I)$  for networks of ground-based interferometers. We consider the following five second-generation interferometers; LIGO-Hanford (H), LIGO-Livingston (L), Virgo (V), KAGRA (K) and LIGO-India (I). For their locations and orientations, we use Table.2 in Schutz (2011). But, for KAGRA, we apply the updated data; the geographical position  $(137.3^\circ\text{E}, 36.4^\circ\text{N})$  and the orientation angle  $74.6^\circ$  for the



**Table 3.** The network parameters  $s_j$  for various networks of ground-based interferometers. We consider up to five interferometers (H: LIGO-Hanford, L: LIGO-Livingston, V: Virgo, K: KAGRA, I: LIGO-India). All of them are assumed to have an identical noise curve. The networks with bold letters are those shown in Fig.6.

network	$s_2$	$s_4$	$s_6$	$s_8$	$s_{10}$
<b>single</b>	1	1	1	1	1
<b>HL</b>	0.910762	0.846346	0.795697	0.753916	0.718351
HV	0.560663	0.410021	0.334791	0.289303	0.258356
VK	0.721165	0.587502	0.504867	0.447881	0.405944
<b>HLV</b>	0.587682	0.421862	0.329701	0.27037	0.228792
<b>HLVK</b>	0.495651	0.311737	0.221355	0.169049	0.135311
HLVI	0.470593	0.29952	0.217136	0.168838	0.137002
<b>HLVKI</b>	0.425877	0.246289	0.164202	0.118532	0.089929

bisector of its two arms measured counter-clock wise from the local East direction. All the detectors are assumed to have identical noise spectrum (and thus the identical horizon distance).

In Table.3, we present the network parameters  $s_j$  for various potential networks composed by the five interferometers. We have the identities  $s_j = 1$  for single interferometer, as mentioned earlier. The two LIGO interferometers H and L are separated by  $\sim 3000$ km but configured to realize large overlaps for incoming GW signals (Cutler & Flanagan 1994). To this end, their orientations are nearly aligned. This results in larger network parameters  $s_j$ , compared with other two-detector networks such as HV or VK.

The five-detector network HLVKI has the smallest network parameters  $s_j$  in Table.3, indicating that due to the randomness of detector configurations, the degree of asymmetry  $\epsilon$  decreases.

In Fig.5, we show the full functions  $P_{net}(I)$  for a single interferometer (dashed curve) as well as the HL, HLV, HLVK and HLVKI networks (solid curves from top to bottom). We use the 12th order approximation for the perturbative expansion. Using *Mathematica*, we can straightforwardly calculate the network parameters  $s_j$  and evaluate the perturbative expressions. As we increase the number of interferometers, the PDF moves from  $P_1(I)$  (for a single interferometer) to  $P_0(I)$ , decreasing fraction of edge-on binaries.

The PDF for the HL network is close to that of a single interferometer, as easily expected from the relatively large network parameters in Table.3. For nearly edge-on binaries ( $I \sim 0$ ), the number of detectable volume depends on  $\psi'$  as  $\propto [1 + \epsilon(\mathbf{n}) \cos 4\psi']^{3/2}$  (see Eq.(5)), and the detected binaries are likely to have polarization angles around  $\psi' = 0 \pmod{\pi/2}$  for the HL network. The PDFs for the HLVKI network is reproduced by Schutz's approximation  $P_0(I)$  with error less than 8%, even around  $I \sim 0$ .

The fraction of nearly edge-on binaries detected by the HLVKI network would be  $\sim 10\%$  smaller than that of the HL network. But we should recall that the emitted GW power (thus the detectable range) is smallest to the edge-on direction  $I \sim 0$ . Indeed, we have the ratio of the emitted powers  $D_0(I = 0)/D_0(I = 1) = 1/8$ , compared with face-on binaries  $I = 1$ . As shown in Fig.2, the nearly edge-on binaries would be a minor component in the whole detected sample.

#### 4.5 Total Detection Rate

So far, we have studied PDFs of inclinations  $I$  (and  $\theta$ ). In this subsection, we go back to §2.3 about the relative detection rate which was analytically examined in Seto (2014). We apply our perturba-

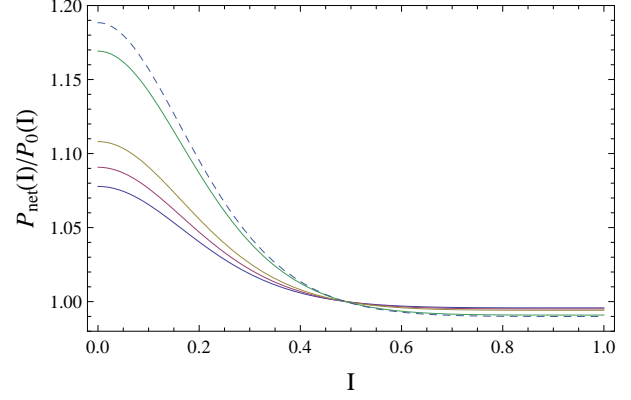


**Figure 6.** The ratios  $P_{net}(I)/P_0(I)$  for various networks. Dashed curve is given for a single detector network and four solid curves are for HL, HLV, HLVK and HLVKI (from top to bottom at  $I = 0$ ).

**Table 4.** The ratio  $Y$  for various networks

single	HL	HLV	HLVK	HLVKI
1.010125	1.00919	1.00588	1.00495	1.00424

tive formulation for the ratio  $Y = X/X_0$  defined in Eq.(28). This ratio represents validity of Schutz's approximation  $X_0$  for estimating the relative detection rates  $X$ .

From Eqs.(44) and (48) we can easily obtain

$$Y = \frac{M_{net}}{N_0} = 1 + \frac{3}{16} \frac{u_2 s_2}{N_0} + \frac{9}{1024} \frac{u_4 s_4}{N_0} + \frac{35}{16384} \frac{u_6 s_6}{N_0} + \dots, \quad (51)$$

and the ratio  $Y$  can be directly evaluated, as actual numbers. In Table.4, we provide them for various networks of detectors, again assuming that all the component detectors have the same sensitivity.

As expected from Table 3, the HL network has the deviation 0.92% close to the maximum value 1.01% for a single detector (see also inequalities (39)). This deviation would be sufficiently small for astronomical arguments, but the deviation for the HLVKI network is further smaller and  $\sim 0.42\%$ .

## 5 SUMMARY

In this paper, we discussed the probability distribution function  $P_{net}(I)$  of inclinations  $I = \cos \theta$  ( $\theta$ : inclination angle) for compact binaries that are detected by a coherent signal analysis with a network of ground-based GW interferometers. In a coherent signal analysis, the SNR of a binary depends not only on its sky direction  $\mathbf{n}$  and inclination  $I$ , but also on its polarization angle  $\psi$ . We have extensively used the simple form (5) given by Cutler and Flanagan (1994) to properly include the  $\psi$ -dependence. Here we have an important parameter  $\epsilon(\mathbf{n})$  that characterizes the asymmetry of the network sensitivities to two orthogonal polarization modes from direction  $\mathbf{n}$ . This parameter has the identity  $\epsilon(\mathbf{n}) = 1$  for a single interferometer and an asymptotic behaviour  $\epsilon(\mathbf{n}) \rightarrow 0$  for large number of randomly placed interferometers. One of the central issues in this paper was how to deal with the effects of the parameter  $\epsilon(\mathbf{n})$ .

Schutz (2011) derived a PDF under a simplification equivalent to setting  $\epsilon(\mathbf{n}) = 0$  in this paper. This simplified PDF corresponds to  $P_0(I)$  defined in Eq.(34), and we showed that it works well for

face-on binaries ( $I = 1$ ) with errors less than  $\sim 1\%$ . On the other hand, for edge-on binaries ( $I = 0$ ), this function is  $\sim 20\%$  smaller than  $P_1(I)$  defined for a single interferometer.

In the cumulative form defined in Eq.(42), the PDF for a given network is reproduced by the simple expression  $\mathcal{P}_{cum}(\theta, 0)$  at  $\sim 1\%$  accuracy. Therefore, the fitting formula (40) and Table.1 would be useful for astronomical arguments such as prospects of EM counterpart searches triggered by GW detections.

We also developed a perturbative method to evaluate the function  $P_{net}(I)$  by introducing the network parameters  $s_j$  ( $j = 2, 4, \dots$ ). These parameters are given by certain angular averages of the moments  $\epsilon(\mathbf{n})^j$ . Convergence of our expansion is fast, and expressions including the first few correction terms of Eqs.(45) and (48) would be sufficient in practice. Even if the horizon distances of individual interferometers are different, we can easily apply our method for arbitrary networks, by introducing appropriate weights for detectors.

We generated the PDFs concretely for the potential networks composed by the second generation detectors. The network with the two LIGO interferometers (HL) has relatively large values  $s_j$ , due to their nearly aligned configurations, and the function  $P_{net}(I)$  is similar to  $P_1(I)$  defined for a single interferometer. On the other hand, the PDF of the network composed by the five interferometers (HLVKI) is closer to  $P_0(I)$  with smaller network parameters  $s_j$ .

The author thanks to H.Tagoshi and K.Kyutoku for helpful conversations. This work was supported by JSPS (24540269) and MEXT (24103006).

## REFERENCES

- Abadie J., et al., 2010, *Class.Quan.Grav*, 27, 173001  
Apostolatos T. A., Cutler C., Sussman G. J., Thorne K. S., 1994, *Phys.Rev.D*, 49, 6274  
Arun K. G., Tagoshi H., Kant Mishra C., Pai A., 2014, arXiv, arXiv:1403.6917  
Berger E., 2013, arXiv, arXiv:1311.2603  
Berger E., Fong W., Chornock R., 2013, *ApJ*, 774, L23  
Blanchet L., Faye G., Iyer B. R., Sinha S., 2008, *Class.Quan.Grav*, 25, 165003  
Cannon K., et al., 2012, *ApJ*, 748, 136  
Cutler C., Flanagan É. E., 1994, *Phys.Rev.D*, 49, 2658  
Dietz A., Fotopoulos N., Singer L., Cutler C., 2013, *Phys.Rev.D*, 87, 064033  
Evans P. A., et al., 2012, *ApJS*, 203, 28  
Fairhurst S., 2011, *Class.Quan.Grav*, 28, 105021  
Finn L. S., Chernoff D. F., 1993, *Phys.Rev.D*, 47, 2198  
Ghosh S., Bose S., 2013, arXiv, arXiv:1308.6081  
Hotokezaka K., Kyutoku K., Tanaka M., Kiuchi K., Sekiguchi Y., Shibata M., Wanajo S., 2013, *ApJ*, 778, L16  
Kelley L. Z., Mandel I., Ramirez-Ruiz E., 2013, *Phys.Rev.D*, 87, 123004  
Kyutoku K., Ioka K., Shibata M., 2014, *MNRAS*, 437, L6  
Kyutoku K., Seto N., 2014, *MNRAS*, 441, 1934  
LIGO Scientific Collaboration, et al., 2013, arXiv, arXiv:1304.067  
Metzger B. D., Berger E., 2012, *ApJ*, 746, 48  
Nakar E., 2007, *Phy.Rep*, 442, 166  
Nissanke S., Holz D. E., Hughes S. A., Dalal N., Sievers J. L., 2010, *ApJ*, 725, 496  
Nissanke S., Kasliwal M., Georgieva A., 2013, *ApJ*, 767, 124  
Peters P. C., Mathews J., 1963, *Phys.Rev.*, 131, 435

- Piran T., Nakar E., Rosswog S., 2013, *MNRAS*, 430, 2121  
Sathyaprakash B. S., Schutz B. F., 2009, *Liv.Rev.Rel*, 12, 2  
Schutz B. F., 2011, *Class.Quan.Grav*, 28, 125023  
Seto, N., 2014, arXiv, arXiv:1406.4238  
Tagoshi H., Kant Mishra C., Pai A., Arun K. G., 2014, arXiv, arXiv:1403.6915  
Tanvir N. R., Levan A. J., Fruchter A. S., Hjorth J., Hounsell R. A., Wiersema K., Tunnicliffe R. L., 2013, *Natur*, 500, 547  
Van Den Broeck C., Sengupta A. S., 2007, *Class.Quan.Grav*, 24, 155